Numerically discovered inherent states are always protocol dependent in jammed packings

Eddie Bautista [*] and Eric I. Corwin [†]
Department of Physics and Materials Science Institute, University of Oregon, Eugene, Oregon 97403, USA

(Received 2 September 2025; revised 27 January 2026; accepted 20 February 2026; published 3 April 2026)

The energy landscape for soft sphere packings exists in a high-dimensional space and plays host to an astronomical number of local minima in a hierarchical and ultrametric arrangement. Each point in the landscape is a configuration that can be mapped to its inherent state, defined as the local minima that the configuration will flow to under perfectly overdamped continuous dynamics. Typically, discrete in time dynamics are used to computationally find local minima, but it is not known whether these algorithms are capable of reliably finding inherent states. Here, we use steepest descent dynamics to find the distribution of the largest time step, δ_{best}, which finds the inherent state. We find that δ_{best} is Weibull distributed. Additionally, for systems of N particles, δ_{best} falls rapidly with increasing N, with a functional form somewhere in between an exponential and inverse power law, and is weakly dependent on d and φ, where d is the packing dimension and φ is the packing fraction. We argue that this rapid fall is due to saddle points in the energy landscape. Our results suggest that it is impossible, in practice, to reliably find inherent states for systems of about 64 particles or more.

DOI: 10.1103/fg38-mtlf

I. INTRODUCTION

In finite dimensions, granular packings of soft spheres are thought to exist in a low-density unjammed phase and a high-density jammed Gardner phase [1,2]. Separating them is the jamming transition, a random first-order, athermal phase transition [2–9]. Signatures of a fractally rough landscape have been seen in finite-dimensional granular packings [10–13]. Thus, the energy landscape in the low-density phase is simple and smooth, while that of the high-density phase consists of a fractally rough set of hierarchical sub-basins within sub-basins *ad infinitum* playing host to an astronomical number of local minima [5,10,14–19].

Each point in the high-density landscape can be unambiguously mapped to its "inherent state," which is defined as the local minima that the configuration will flow to under perfectly overdamped continuous dynamics [20–24]. These dynamics are often approximated with various discrete in time dynamics in order to computationally approximate the inherent state. This mapping segments the landscape into individual basins of attraction [21,25]. This segmentation of space allows one to define the Shannon entropy for the landscape, which is expected to control thermodynamic and statistical mechanical properties of granular packings [21,26]. The typical method for finding inherent states is to choose a time step (or equivalent scale) for which the resulting minima are insensitive. However, it is not known whether such methods can reliably and reproducibly find the true inherent state for all starting configurations. In this work, we demonstrate that, for sufficiently large systems, they cannot. This suggests that prior work relying on inherent states should be revisited. These results place a computational limit on the use of the basin of attraction method to study glasses.

Here, we sample the energy landscape and flow to local minima using steepest descent dynamics with systematically varying time steps. We find that for every starting configuration, there exists some time step above which the system falls into a minima other than the inherent state. We find that the value of this time step needed to find the inherent state decays rapidly with particle number and is only weakly dependent on packing fraction φ and spatial dimension d. We argue that the strong correlation between time step and particle number is due to saddle points in the fractally rough energy landscape. We find that these constraints place limits on the computability of inherent states, under any circumstances, to systems of about $N = 64$ particles or fewer.

Many discrete numerical algorithms exist to find local minima in the landscape. Some examples include CVODE [27,28], the fast inertial relaxation engine (FIRE) [29,30], the limited memory Broyden-Fletcher-Goldfarb-Shanno (L-BFGS) scheme [31], and Steepest Descent [32]. Some momentum-based algorithms, such as FIRE and L-BFGS, have already been found to incorrectly identify inherent states due to the introduction of an effective "noise" in the energy landscape [33,34]. This noise causes the packings to jump over small barriers in the landscape into neighboring minima. In this work, we show that even first-order iterative algorithms such as Steepest Descent are only able to find the inherent state when using extremely small step sizes. We use the steepest descent minimizer because it is the simplest and best understood minimizer, thus ensuring any behavior we find is due to the energy landscape and not the complexities of the minimizer.

II. MODEL

We simulate N harmonic soft spheres in a d-dimensional box of side length 1 with periodic boundary conditions. The total energy of a system composed of spheres with locations

[*]Contact author: ebautis2@uoregon.edu
[†]Contact author: ecorwin@uoregon.edu

$\{\vec{x}_i\}$ and radii $\{r_i\}$ is defined as

$$U(\{\vec{x}_i\}) = \frac{1}{2}\sum_{ij}\left(1 - \frac{\|\vec{x}_i - \vec{x}_j\|}{r_i + r_j}\right)^2 \Theta\left(1 - \frac{\|\vec{x}_i - \vec{x}_j\|}{r_i + r_j}\right), \tag{1}$$

where Θ is the Heaviside function necessary for a contact potential. In this work, we chose a harmonic potential, which is not infinitely differentiable at the points of contact. At large packing fractions, and far away from contact changes, this potential behaves analytically. As such, we expect our results to apply broadly to the kinds of contact potentials relevant to jamming. However, future work should explore the extent to which the results presented here may be affected by the (non)analyticity of the energy landscape, perhaps using the spherical p-spin model as an example of an analytic landscape.

The dynamics to reach an inherent state are defined as

$$\frac{\partial\{\vec{x}_i\}}{\partial t} = -\nabla U(\{\vec{x}_i\}). \tag{2}$$

We discretize these dynamics to form a steepest descent (SD) minimizer with a fixed time step δ as

$$\{\vec{x}_{i,t+1}\} = \{\vec{x}_{i,t}\} - \delta\nabla U(\{x_{i,t}\}), \tag{3}$$

where $\{\vec{x}_i, t\}$ is the position of all particles at time step t. Throughout the minimization, δ is kept constant.

III. METHODS

An energy landscape is uniquely defined by the packing spatial dimension d, particle number N, and the set of particle radii $\{r_i\}$. To prevent crystallization in $d = 2$, we use radii drawn from a log-normal distribution with a polydispersity (ratio of standard deviation to mean) equal to 0.25. In higher dimensions, we use monodisperse radii, as there is no spontaneous crystallization. For a given landscape, we sample 1000 random initial states uniformly across the space. We choose to start at random initial states, which can be interpreted as infinite-temperature configurations, so that we can employ a flat measure across the entire energy landscape.

For each initial state, we minimize the packing energy using the steepest descent dynamics in Eq. (3) as implemented by the PYCUDAPACKING software [35–37], a GPU-based sphere packing minimizer. We use time steps ranging from $\delta = 10^{-6}$ to 10^{-2} in natural units. We chose 10^{-6} as our lower limit because of time and resource constraints. Steps larger than 10^{-2} tend to overshoot minima or diverge at high rates, therefore making them unsuitable for exploration.

For each choice of δ, a given initial configuration can, in principle, minimize to a different final state in the energy landscape. However, many values of δ will minimize the initial state to the same minimum, as shown in Fig. 1. To determine whether two minima are the same, we find that it is sufficient to compare their energies [38]; if the energies differ by less than 10^{-10} we can be confident that the systems are in the same minima. In $d = 2$, we verify this by looking at the contact vector distance to identify minima, as was done in Ref. [10]. This verification only works in $d = 2$ because the radii are polydispersed; thus, the particles are distinguishable.

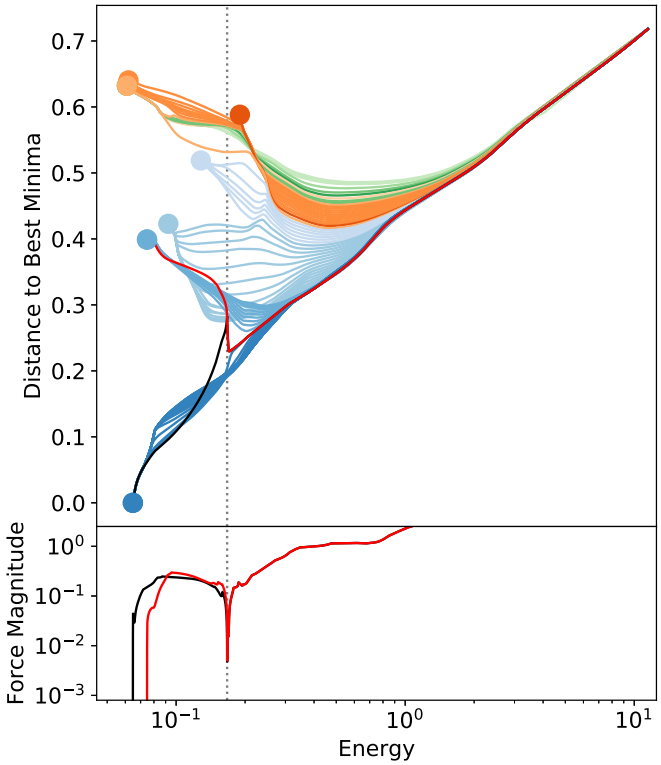

FIG. 1. Top: Steepest descent minimization paths using varying time steps starting from the same initial state. We minimize the initial packing using time steps δ between 10^{-6} and 10^{-2}. Each line represents the SD path of a different δ, colored according to the unique minima to which the state will flow. The top green line is our largest time step, with each subsequent line below it representing smaller and smaller time steps. The final states are indicated by circle markers. We see the curves naturally segment themselves based on the time step. The black and red curves show the path for δ's right above and right below δ_{crit} for the saddle point separating the best minima and its first neighbor. We see the paths stick closely together until the saddle point energy, at which they separate sharply. Bottom: Force plot for the black and red curves. At the point of separation, indicated by the black dotted line, we see a drastic dip in the force. This tells us that it is a saddle point in the energy landscape.

Ideally, we would compare the minima found with a given value of δ to the true inherent state. However, lacking any scheme to produce such an inherent state, we instead define the "best minima" as the minima found using the smallest practicable time step, 10^{-6}.

For a given starting point, we determine δ_{best}, the largest time step such that all smaller time steps result in the best minima. The value δ_{best} gives us insight into how small a time step is needed to be reasonably sure we have found the inherent state. To see how δ_{best} changes, we sample packings in $d = 2$, 3, and 4 spatial dimensions with different particle numbers N, and packing fractions φ.

IV. RESULTS

In order to understand how the discrete-time dynamics influence the trajectory of a system, we look at the steepest descent path. For a given starting configuration, we first find

the best minima using $\delta = 10^{-6}$. Then, for a range of values of δ logarithmically spaced up to 10^{-2}, we record, at every minimization time step, the energy, force magnitude, and distance in position space to the best minima.

Figure 1 (top) shows these discrete-time steepest descent paths for a $d = 2$ packing of $N = 16$ particles at $\varphi = 1.07\varphi_J$, where φ_J is the jamming packing fraction. Each line represents a different time step, and the color represents into which unique minima the packing minimizes. We see that for time steps lower than $\sim 5 \times 10^{-3}$, the lines are well segmented by color, meaning that there is a continuous range of δ for which the SD dynamics all minimize to the same minima. The value of δ which separates each adjacent range of time steps is a critical time step δ_{crit} whose dynamics bring the system not to a minima, but to a saddle point which separates those two minima.

For energy landscapes in high-dimensional spaces, low-index saddle points are attractive in all but a small number of directions. Thus, the trajectory of a perfectly overdamped continuous dynamics will approach closely to each saddle point that it encounters on the way down to the inherent state. Further, in high dimensions, a random initial state is likely to be near a border between basins of attraction in the energy landscape and so the perfectly overdamped trajectory of such a state will follow the border towards a saddle [39]. The time step in discrete-time SD dynamics introduces an effective momentum, which allows the system to deviate from the perfectly overdamped path. With enough momentum and close to a saddle point, the system can be carried over the separatrix between neighboring minima. Previous work has shown the importance of saddles in the energy landscape of glassy materials [40–44].

We can verify these are indeed saddle points by first adjusting δ so that the minimization path comes arbitrarily close to the separatrix between wells. The black and red lines in Fig. 1 (top) are the paths for time steps bracketing δ_{crit} for a representative saddle point. The red curve has $\delta = \delta_{\text{crit}} + 10^{-20}$ and the black curve has $\delta = \delta_{\text{crit}} - 10^{-20}$. We see that the paths are identical until they hit the saddle point, whose energy is indicated by the dashed vertical line, at which point they abruptly begin to separate. Figure 1 (bottom) shows the force versus energy plot of the black and red curves. At the saddle point, there is a sudden dip in the force towards zero, consistent with a critical point. Examining the Hessian reveals that it is an index one saddle point, meaning that there is a single repulsive eigenvector for the associated dynamical, or Hessian, matrix, and all other eigenvectors are attracted to the saddle point.

For a given starting configuration, we can thus see that

$$\delta_{\text{best}} = \min[\{\delta_{\text{crit},i}\}], \tag{4}$$

where $\{\delta_{\text{crit},i}\}$ is the set of saddle points encountered by the minimization path. As δ_{best} is bounded from below by zero, one should expect the resulting δ_{best} to be distributed according to a Weibull distribution [45,46] with centering and width determined by the functional form of the lower tail of the distribution of δ_{crit}. In fact, under certain circumstances, one might find a Gumbel distribution instead, but this proves a poor fit to our measured data and so is not explored here. When measured with respect to the true inherent state, we

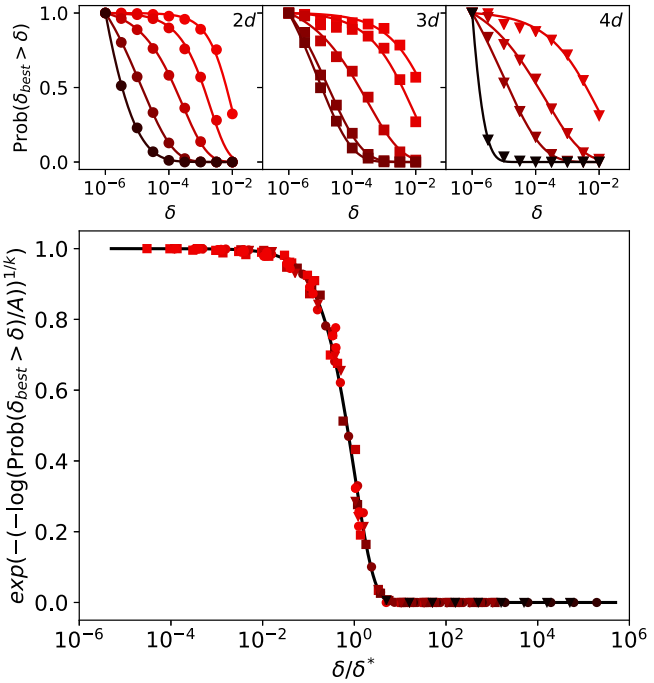

FIG. 2. Top: Complementary cumulative distribution function of δ_{best} for packings in $d = 2$ (left), $d = 3$ (middle), and $d = 4$ (right) spatial dimensions with changing N and φ held constant at $1.07\varphi_J$. The y axis shows the probability that δ_{best} is above a given time step δ. The colors represent different N with darker colors conveying larger particle numbers. The lines show the fits to the complementary cumulative distribution function of the Weibull distribution, Eq. (6). Bottom: Scaled complementary cumulative distribution function for all data in the top figure. The x axis is scaled by δ^*, and the y axis has the A and k parameters scaled out. The circles represent the $d = 2$ data, the squares $d = 3$, and the triangles $d = 4$. Also included are $d = 2, N = 16$ packings with $\varphi = 1.01\varphi_J$ and $1.13\varphi_J$.

should then find δ_{best} distributed according to

$$f(\delta; \delta^*, k) = \frac{k}{\delta^*}\left(\frac{\delta}{\delta^*}\right)^{k-1} e^{-(\delta/\delta^*)^k}, \tag{5}$$

where k is the shape parameter and δ^* is the scale parameter.

This picture is complicated by the fact that the measured value of δ_{best} is *not* the value below which the system will always minimize to the true inherent state, but rather the value below which the system will always minimize to the same minimum as when $\delta = 10^{-6}$. This can be incorporated into a prediction for the complementary cumulative distribution of the measured δ_{best} as a truncated Weibull,

$$\text{Prob}(\delta_{\text{best}} > \delta) = Ae^{-(\delta/\delta^*)^k}, \tag{6}$$

where k and δ^* are the same shape and scale parameter as in Eq. (5) and $A = \exp[(10^{-6}/\delta^*)^k]$ is a normalization factor to enforce $\text{Prob}(\delta_{\text{best}} > 10^{-6}) = 1$.

Figure 2 (top) Shows the complementary cumulative distribution function of δ_{best} for $d = 2$ (left), $d = 3$ (middle), and $d = 4$ (right) packings with $\varphi = 1.07\varphi_J$. The y axis shows the probability of finding the best minima using time step δ. Each color represents a different particle number, and each line shows the fits to the complementary cumulative

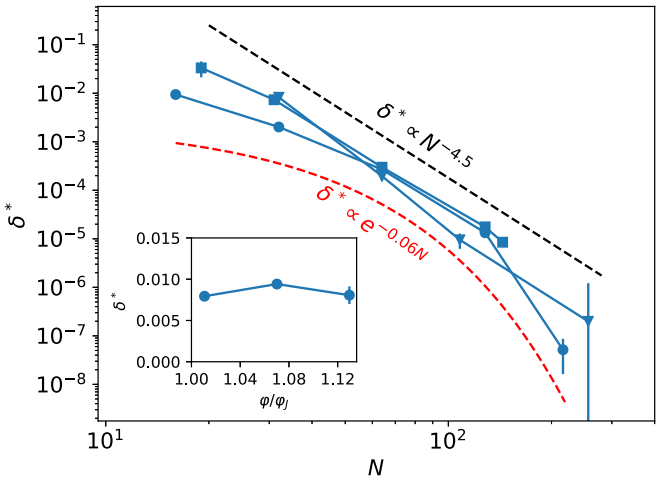

FIG. 3. Log-log plot of δ^* as a function of particle number for $d = 2$, 3, and 4 spatial dimensions at packing fractions of $1.07\varphi_J$. The circles represent the $d = 2$ data, the squares $d = 3$, and the triangles $d = 4$. The black dashed line shows a power-law decay, while the red dashed line shows an exponential decay. Over this range, we see δ^* fall with a functional form in between an exponential and an inverse power law. In the inset, we show δ^* as a function of packing fraction for a $d = 2$ packing with $N = 16$. Here, we see δ^* is nearly independent of φ. The error bars are due to fitting.

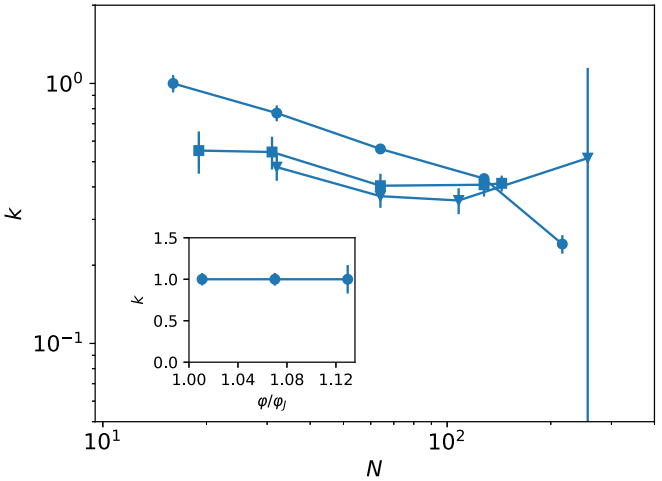

FIG. 4. Log-log plot of k, the Weibull shape parameter, as a function of particle number for $d = 2$, 3, and 4 spatial dimensions at a packing fraction of $1.07\varphi_J$. Circle markers represent $d = 2$, square markers $d = 3$, and triangles $d = 4$. In the inset, we show k as a function of packing fraction for a $d = 2$, $N = 16$ packing. The error bars are due to fitting.

distribution function. In $d = 2$, $N = 16$, 32, 64, 128, 216. In $d = 3$, $N = 19$, 31, 64, 128, 144. Finally, in $d = 4$, $N = 32$, 64, 108, 256. For a given value of N we find that this probability falls monotonically with increasing values of δ.

Additionally, we look at the distribution of δ_{best} for the $d = 2, N = 16$ packings at $\varphi = 1.01\varphi_J$ and $1.13\varphi_J$. As shown in Fig. 2 (bottom), every d, N, and φ distribution can be collapsed onto a master curve by scaling the x axis by δ^* and scaling out the A and k parameters from the y axis. All data collapse well to this master curve, affirming that δ_{best} is indeed Weibull distributed.

Figure 3 shows δ^*, the characteristic time step of the distribution, as a function of particle number on a log-log plot for packings in $d = 2$, 3, and 4 spatial dimensions. All packings are at a packing fraction of $1.07\varphi_J$. We see that over this, admittedly limited, range in particle number, δ^* falls with a functional form somewhere in between an exponential and an inverse power law. Thus, there is a sharp dropoff in δ_{best} with increasing N, meaning we have to go to increasingly smaller time steps as we gradually increase the particle number. As a result, it is practically impossible to reliably find inherent states for systems of more than about 64 particles.

When applying our methods to systems larger than those studied here, we found that δ_{best} was always the smallest δ tried. Thus, it would be necessary to search for ever smaller time steps, which become computationally infeasible. Therefore, we cannot derive any meaningful statistics about δ_{best} for larger systems. However, this does ably demonstrate that larger particle numbers do, in fact, require smaller time steps.

The inset in Fig. 3 shows δ^* as a function of φ for a $d = 2$ packing with $N = 16$. Here, we see that δ^* is nearly independent of φ.

Figure 4 shows k, the Weibull shape parameter, as a function of particle number on a log-log plot for $d = 2$, 3, and 4 packings. As before, all packings were held at a constant packing fraction of $1.07\varphi_J$. We see only a gentle decrease in k with increasing N. In the inset in Fig. 4, we show k as a function of φ for a $d = 2$ packing with $N = 16$. We see over this range of φ that k is nearly independent of φ.

V. CONCLUSION

These results demonstrate that it is virtually impossible to find inherent states for granular packings of large numbers of particles (in our case, 64 particles or more). This is because the steepest descent paths are attracted to saddle points in the energy landscape, each of which has an associated critical time step δ_{crit} above which the system will be shunted into the wrong minimum. In order to find the true inherent state, one must choose a time step δ that is lower than the smallest δ_{crit}. The set of time steps leading to inherent states is Weibull distributed, and their centering falls rapidly with N, more quickly than a power law but slower than an exponential. This centering is seemingly independent of d and φ.

These results indicate that the problem of finding inherent states is not just due to computational precision, but rather a physical one having to do with saddle points in the energy landscape. The Weibull distribution of δ_{best} further goes on to relate this phenomenon to the extreme value problem of choosing a time step smaller than the saddle point with the smallest δ_{crit} along the perfectly overdamped continuous dynamics path.

Adaptive minimization algorithms that change the time step as they minimize can speed up the beginning of the minimization process, thus allowing one to employ smaller time steps δ. However, we still must go to extremely small time steps to find the inherent state. Most of the computational effort will be spent close to these saddle points and using very small time steps; therefore, the adaptive algorithms will likely have only a marginal effect on the computational resources

needed to accurately find the inherent state for large systems. Thus, the framework of the inherent state tessellation of space, while conceptually attractive, seems to be impractical. An additional complication with adaptive algorithms comes from the fact that the jamming landscape is fractal in nature. This means that no matter where the packing may be along the path (i.e., how thermally equilibrated it is), for sufficiently large systems, the packing will always encounter a large number of saddle points and will have to make choices based on the time step. Since the problem presented here is a physical one, every algorithm, despite how sophisticated it may be, will encounter the extreme value problem.

Our article suggests that much of the work relying on accurately identifying inherent states of glassy materials needs to be revisited. Additionally, we show how extreme value statistics can affect the dynamics of jammed packings. This result allows us to use extreme value methods to study the energy landscape of glassy materials, thus opening another avenue of study.

ACKNOWLEDGMENTS

We thank Cam Dennis, Peter Morse, Jorge Kurchan, Giorgio Parisi, Sean Ridout, and Ivan Corwin for useful discussions. This work was supported by a grant from the Simons Foundation No. 454939. The simulations were performed on the University of Oregon high-performance computing cluster, Talapas.

DATA AVAILABILITY

The data that support the findings of this article are openly available [47], embargo periods may apply.

[1] L. Berthier, G. Biroli, P. Charbonneau, E. I. Corwin, S. Franz, and F. Zamponi, Gardner physics in amorphous solids and beyond, J. Chem. Phys. **151**, 010901 (2019).

[2] T. Castellani and A. Cavagna, Spin-glass theory for pedestrians, J. Stat. Mech. (2005) P05012.

[3] A. J. Liu and S. R. Nagel, Jamming is not just cool any more, Nature (London) **396**, 21 (1998).

[4] L. Berthier, D. Coslovich, A. Ninarello, and M. Ozawa, Equilibrium sampling of hard spheres up to the jamming density and beyond, Phys. Rev. Lett. **116**, 238002 (2016).

[5] P. Charbonneau, J. Kurchan, G. Parisi, P. Urbani, and F. Zamponi, Glass and jamming transitions: From exact results to finite-dimensional descriptions, Annu. Rev. Condens. Matter Phys. **8**, 265 (2017).

[6] M. D. Rintoul and S. Torquato, Metastability and crystallization in hard-sphere systems, Phys. Rev. Lett. **77**, 4198 (1996).

[7] P. Charbonneau, E. I. Corwin, R. C. Dennis, R. Díaz Hernández Rojas, H. Ikeda, G. Parisi, and F. Ricci-Tersenghi, Finite-size effects in the microscopic critical properties of jammed configurations: A comprehensive study of the effects of different types of disorder, Phys. Rev. E **104**, 014102 (2021).

[8] F. Arceri, E. I. Corwin, and C. S. O'Hern, The jamming transition and the marginally stable solid, *Spin Glass Theory & Far Beyond–Replica Symmetry Breaking After 40 Years* (World Scientific, 2023).

[9] T. Bertrand, R. P. Behringer, B. Chakraborty, C. S. O'Hern, and M. D. Shattuck, Protocol dependence of the jamming transition, Phys. Rev. E **93**, 012901 (2016).

[10] R. C. Dennis and E. I. Corwin, Jamming energy landscape is hierarchical and ultrametric, Phys. Rev. Lett. **124**, 078002 (2020).

[11] A. P. Hammond and E. I. Corwin, Experimental observation of the marginal glass phase in a colloidal glass, Proc. Natl. Acad. Sci. USA **117**, 5714 (2020).

[12] A. Seguin and O. Dauchot, Experimental evidence of the gardner phase in a granular glass, Phys. Rev. Lett. **117**, 228001 (2016).

[13] L. Kool, P. Charbonneau, and K. E. Daniels, Gardner-like crossover from variable to persistent force contacts in granular crystals, Phys. Rev. E **106**, 054901 (2022).

[14] C. Artiaco, P. Baldan, and G. Parisi, An exploratory study of the glassy landscape near jamming, Phys. Rev. E **101**, 052605 (2020).

[15] P. Charbonneau, J. Kurchan, G. Parisi, P. Urbani, and F. Zamponi, Exact theory of dense amorphous hard spheres in high dimension. III. The full RSB solution, J. Stat. Mech. (2014) P10009.

[16] P. Charbonneau, J. Kurchan, G. Parisi, P. Urbani, and F. Zamponi, Fractal free energy landscapes in structural glasses, Nat. Commun. **5**, 3725 (2014).

[17] A. Thirumalaiswamy, R. A. Riggleman, and J. C. Crocker, Exploring canyons in glassy energy landscapes using metadynamics, Proc. Natl. Acad. Sci. USA **119**, e2210535119 (2022).

[18] C. Rainone, P. Urbani, H. Yoshino, and F. Zamponi, Following the evolution of hard sphere glasses in infinite dimensions under external perturbations: Compression and shear strain, Phys. Rev. Lett. **114**, 015701 (2015).

[19] P. Urbani and F. Zamponi, Shear yielding and shear jamming of dense hard sphere glasses, Phys. Rev. Lett. **118**, 038001 (2017).

[20] F. Sciortino, Potential energy landscape description of supercooled liquids and glasses, J. Stat. Mech. (2005) P05015.

[21] S. Martiniani and M. Casiulis, When you can't count, sample! Computable entropies beyond equilibrium from basin volumes, Pap. Phys. **15**, 150001 (2023).

[22] R. J. Speedy, Random jammed packings of hard discs and spheres, J. Phys.: Condens. Matter **10**, 4185 (1998).

[23] S. Martiniani, K. J. Schrenk, J. D. Stevenson, D. J. Wales, and D. Frenkel, Structural analysis of high-dimensional basins of attraction, Phys. Rev. E **94**, 031301(R) (2016).

[24] G.-J. Gao, J. Blawzdziewicz, and C. S. O'Hern, Enumeration of distinct mechanically stable disk packings in small systems, Philos. Mag. **87**, 425 (2007).

[25] S. S. Ashwin, J. Blawzdziewicz, C. S. O'Hern, and M. D. Shattuck, Calculations of the structure of basin volumes for mechanically stable packings, Phys. Rev. E **85**, 061307 (2012).

[26] S. Martiniani, K. J. Schrenk, K. Ramola, B. Chakraborty, and D. Frenkel, Numerical test of the edwards conjecture shows that all packings are equally probable at jamming, Nat. Phys. **13**, 848 (2017).

[27] A. C. Hindmarsh, P. N. Brown, K. E. Grant, S. L. Lee, R. Serban, D. E. Shumaker, and C. S. Woodward, SUNDIALS: Suite of nonlinear and differential/algebraic equation solvers, ACM Trans. Math. Softw. **31**, 363 (2005).

[28] D. J. Gardner, D. R. Reynolds, C. S. Woodward, and C. J. Balos, Enabling new flexibility in the sundials suite of nonlinear and differential/algebraic equation solvers, ACM Trans. Math. Softw. **48**, 31 (2022)0098-3500.

[29] E. Bitzek, P. Koskinen, F. Gähler, M. Moseler, and P. Gumbsch, Structural relaxation made simple, Phys. Rev. Lett. **97**, 170201 (2006).

[30] G. Parisi, P. Urbani, and F. Zamponi, *Theory of Simple Glasses: Exact Solutions in Infinite Dimensions*, 1st ed. (Cambridge University Press, Cambridge, UK, 2020).

[31] D. C. Liu and J. Nocedal, On the limited memory BFGS method for large scale optimization, Math. Program. **45**, 503 (1989).

[32] M. A. Cauchy, Méthode générale pour la résolution des systeèmes d'équations simultanées, C. R. Hebd. Seances Acad. Sci. **25**, 536 (1847).

[33] P. Suryadevara, M. Casiulis, and S. Martiniani, The basins of attraction of soft sphere packings are not fractal, arXiv:2409.12113.

[34] P. Charbonneau and P. K. Morse, Jamming, relaxation, and memory in a minimally structured glass former, Phys. Rev. E **108**, 054102 (2023).

[35] P. K. Morse and E. I. Corwin, Geometric signatures of jamming in the mechanical vacuum, Phys. Rev. Lett. **112**, 115701 (2014).

[36] P. Charbonneau, E. I. Corwin, G. Parisi, A. Poncet, and F. Zamponi, Universal non-debye scaling in the density of states of amorphous solids, Phys. Rev. Lett. **117**, 045503 (2016).

[37] P. K. Morse and E. I. Corwin, Echoes of the glass transition in athermal soft spheres, Phys. Rev. Lett. **119**, 118003 (2017).

[38] V. F. Hagh and S. R. Nagel, Order in disordered packings with and without permutation symmetry, arXiv:2403.03926.

[39] J. Kurchan and L. Laloux, Phase space geometry and slow dynamics, J. Phys. A: Math. Gen. **29**, 1929 (1996).

[40] T. S. Grigera, A. Cavagna, I. Giardina, and G. Parisi, Geometric approach to the dynamic glass transition, Phys. Rev. Lett. **88**, 055502 (2002).

[41] A. Cavagna, I. Giardina, and G. Parisi, Numerical study of metastable states in ising spin glasses, Phys. Rev. Lett. **92**, 120603 (2004).

[42] A. Cavagna, I. Giardina, and G. Parisi, Stationary points of the Thouless-Anderson-Palmer free energy, Phys. Rev. B **57**, 11251 (1998).

[43] A. Cavagna, Fragile vs strong liquids: A saddles-ruled scenario, Europhys. Lett. **53**, 490 (2001).

[44] A. Cavagna, I. Giardina, and G. Parisi, Role of saddles in mean-field dynamics above the glass transition, J. Phys. A: Math. Gen. **34**, 5317 (2001).

[45] W. Weibull, A statistical distribution function of wide applicability, J. Appl. Mech. **18**, 293 (1951)

[46] S. N. Majumdar, A. Pal, G. Schehr, Extreme value statistics of correlated random variables: A pedagogical review, Phys. Rep. **840**, 1 (2020).

[47] E. Bautista and E. I. Corwin, Directory of the initial amorphous granular packing configuration and final amorphous granular packing configuration after minimizing using time step delta with an SD minimizer [Dataset], Dryad (2026), https://doi.org/10.5061/dryad.qjq2bvqv3.